Chem Soc Rev

Multiple Roles of Graphene in Heterogeneous Catalysis

Chem Soc Rev

Chemical Society Reviews

REVIEW ARTICLE

Multiple roles of graphene in heterogeneous catalysis

Xiaobin Fan*[abc], Guoliang Zhang[a] and Fengbao Zhang[a]

5 Scientific interest in graphene as a catalyst and as a catalyst support in heterogeneous catalytic reactions has grown dramatically over the past several years. The present *critical review* summarizes the multiple roles of graphene in heterogeneous catalysis and highlights the influence of defects, heteroatom-containing functionalities, and graphene's two-dimensional structures on catalytic performance. We first discuss the role and advantages of graphene as a catalyst support, with emphasis on their interactions with
10 the catalytic phases and the influence of mass transfer processes. We then clarify the origin of the intrinsic catalytic activity of graphene in heterogeneous catalytic reactions. Finally we suggest challenges and potential practical applications for graphene in industrial processes.

1. Introduction

15 Heterogeneous catalysis is of paramount importance in the chemical and pharmaceutical industry, as well as in energy conversion, environmental treatment and materials science. It is estimated that ~90% of all chemical processes involve heterogeneous catalysis.[1] Carbon plays diverse roles in various
20 heterogeneous catalytic reactions.[2] For example, traditional carbon materials are widely used as catalyst supports in heterogeneous catalysis, especially the supported noble metal catalysts in organic synthesis and in fuel cell electrocatalysis.[3] In addition, carbon is itself a well-known heterogeneous catalyst and
25 is used industrially in selective oxidation, chlorination, dechlorination, and other reactions.[2]

Xiaobin Fan is currently a professor at Tianjin University, China. He received his BSc in
30 *2003 from Nankai University with the major of chemistry. Then he received his MSc and PhD from Department of Chemical Engineering, Tianjin*
35 *University in 2006 and 2009, respectively. He joined Tianjin University in 2009 as a lecturer and got promotion to be an associate professor and*
40 *professor in 2011 and 2013, respectively. His research interests include the preparation and applications of new nanomaterials and green chemistry.*

As the basic building block of carbon nanotubes and many
45 other carbon allotropes,[4] graphene constitutes a two-dimensional (2D) sheet of sp^2-hybridized carbon atoms and has many unique properties. For example, pristine graphene has a remarkably high electron mobility of ~10,000 cm^2 V^{-1} s^{-1} at room temperature,[5] white light absorbance of 2.3% with negligible reflectance,[6]
50 thermal conductivity of 3000–5000 W m^{-1} K^{-1} at room temperature,[7] a Young's modulus of 1 TPa,[8] and a theoretical specific surface area of 2630 m^2 g^{-1}.[9] These exceptional properties endow graphene with great potential for applications in a range of fields.[10-25] In particular, there has been exponential
55 growth in the number of studies on the applications of graphene and its derivatives in heterogeneous catalysis. These materials have emerged as unparalleled 2D supports and catalysts for diverse catalytic reactions. Many excellent studies related to the catalytic applications of graphene, including graphene-based
60 electrocatalysts,[12, 13, 19] metal-free catalysts,[26] photocatalysts,[27] and supercapacitors[28] have been reported. However, most of the applied studies have been carried out using the less expensive and more readily available graphene oxide or the reduced graphene oxide (r-GO) counterpart. Defects and heteroatom-containing
65 functionalities introduced into the graphene basal plane and/or edges by oxidation and/or reduction significantly alter the physical and chemical properties of pristine graphene. For example, the sheet resistance values of graphene oxide are about 1000 Ω sq^{-1} or higher,[29] though the conductivity of r-GO is
70 expected to be ~1000 S m^{-1}.[30] Conversely, the presence of such defects and functional groups can provide potential advantages including good dispersibility in solvents[31] and contribute to the catalytic performance of graphene-based catalysts.[32]

In this review, we highlight the advantages of the 2D structure
75 of graphene and clarify the influences of defects and heteroatom-containing functionalities on its catalytic performance. We aim to

provide a succinct but comprehensive understanding of the different roles of graphene in heterogeneous catalysis (**Scheme 1**), *i.e.*, its use as a catalyst support and its intrinsic catalytic properties.

5
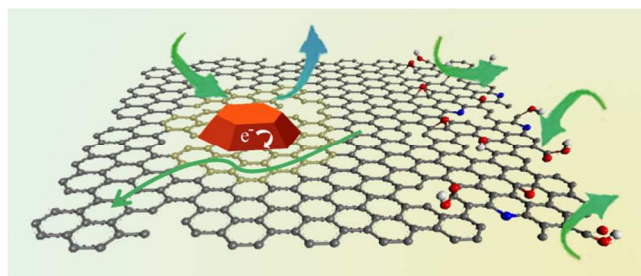
Scheme 1 Illustration of the different roles of graphene in heterogeneous catalysis, *i.e.*, its use as a catalyst support and its intrinsic catalytic properties originating from the defects and heteroatom-containing functionalities.

10 2.   Graphene as a catalyst support

Supported catalysts are the most important type of catalyst in heterogeneous catalyst.[33] Among various supports used in heterogeneous catalysis, carbon materials are attracting growing interest owing to their large surface area and chemical stability,
15 which facilitate high loading of active sites and contribute to their resistance to degradation in both acidic and basic media. In addition, recovering the active phase (especially for the supported noble metal catalysts) is convenient by direct combustion of the carbon supports. Therefore, diverse carbon materials like
20 activated carbon, carbon black and carbon nanotubes have been exploited as catalyst supports.[3]

Compared with other carbon supports, graphene and its derivatives (*e.g.*, graphene oxide) have the unique properties as mentioned above that make them attractive for use in
25 heterogeneous catalysis. Many catalytically active species have been successfully deposited or immobilized on graphene, and the superior catalytic performance of these supported catalysts has been documented in most of the reactions investigated to date. The specific roles and advantages of graphene as a support for
30 catalysts from both chemical and physical perspectives are summarized in this section.

2.1 Interaction with catalytic phases

The intrinsic chemical activity, selectivity, and stability of a supported catalyst not only depend on its composition, structure,
35 size and shape, but also on its interaction with the support.[33] Therefore, great efforts have been made to understand the

interaction between the graphene support and the supported
50 catalytically active species.

For supported metal catalysts, in particular, it is expected that the chemical bonding and associated charge transfer at the interface between the metal particles and support can be used to tune the electronic and chemical properties of the catalytically
55 active sites to achieve higher catalytic activity and selectivity.[33] Furthermore, good dispersion and improved stability of the supported nanoparticles are usually observed in catalysts featuring stronger support interactions. However, graphene is chemically inert because of the strong sp^2 bonding among carbon
60 atoms in the graphene plane that leads to weaker interactions with the supported metal clusters. To address this issue, mechanical strain, defects, and functional groups have been introduced to strengthen the interaction between the catalyst and graphene.
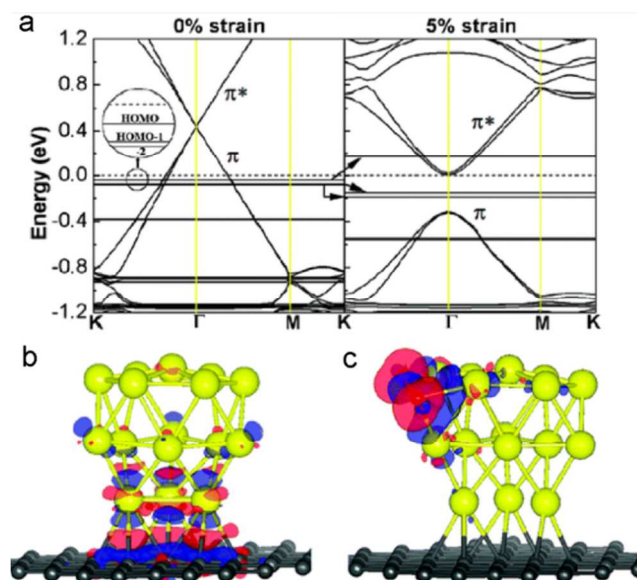

65 **Fig. 1** (a) Band structure of Au_{16}@graphene under zero strain (left panel) and 5% strain (right panel). Inset: Enlarged view of the HOMO, HOMO-1, and HOMO-2 energy levels of Au_{16}, and the Fermi level (dotted line) of the entire system. (b) Isosurface of the differential charge for Au_{16}@graphene when the graphene sheet is under 5% tensile strain, with
70 an isovalue of 0.02 e $Å^{-1}$. The differential charge is calculated as $\Delta\rho = \rho(Au_{16}@graphene) - (\rho(Au_{16}) + \rho(graphene))$. Note that the charge redistribution mainly occurs in the interfacial region. (c) Isosurface of the charge redistribution for an O_2 molecule (red) adsorbed onto Au_{16}@graphene under 5% strain. The differential charge in this case is
75 calculated as $\Delta\rho = \rho(O_2Au_{16}@graphene) - (\rho(O_2) + \rho(Au_{16}@graphene))$. The accumulation (or depletion) of electrons is indicated in red (or blue). Reproduced with permission from ref. 34. Copyright 2010, American Chemical Society.

Guoliang Zhang is currently a professor at Department of Chemical Engineering, Tianjin
40 *University, China. He received his BSc and MSc from Tianjin University in 1982 and 1988, respectively, majoring in chemical engineering. His*
45 *research interests include new nanomaterials and green chemistry.*

Fengbao Zhang is currently a
80 *professor at Department of Chemical Engineering, Tianjin University, China. He received his BSc, MSc and PhD from Tianjin University in 1984, 1987*
85 *and 1991, respectively, majoring in chemical engineering. His research interests include new nanomaterials and green chemistry.*

By using first-principles calculations, Zhang and co-workers[34] reported that the application of a moderate tensile strain to graphene should greatly increases the adsorption energies of different types of metal clusters on graphene. More specifically, in the case of supported Au clusters on graphene for CO oxidation, the strain in graphene reversed the charge transfer between the Au clusters and graphene support, resulting in a significant reduction in the reaction barrier from ~3.0 eV to less than 0.2 eV (**Fig. 1**). However, charge transfer from other metals (*e.g.*, Pt and Cr) to graphene was rarely observed.[35, 36] Only the d band center of the bottommost metal layer could be tuned by external strain on graphene.[35]

Introducing structural defects is a more efficient way to increase the interaction between graphene and the supported catalytic species. As exemplified by Kim and Jhi,[37] the binding of Pt nanoparticles to graphene and the adsorption of target molecules onto Pt could be controlled by introducing defects in graphene. The authors found that the supported Pt nanoparticles were more tolerant toward CO during the hydrogen oxidation reduction of fuel cells. Lim and Wilcox[38] identified strong hybridization of Pt nanoparticles with the sp^2 dangling bonds of neighboring carbon atoms that were close to the monovacancy sites of graphene. The hybridization is expected to enhance the high catalytic performance by preventing the sintering of the Pt nanoparticles and providing a balance in the O_2 binding strength. The formation of Pt−carbon bonds at defects not only affected the average bond length, and thus the strain in the Pt clusters, but also resulted in stronger binding of the clusters to the defective graphene, leading to increased charge transfer and substantial downshift of the d band center of the Pt clusters.[39] Though the trapping ability of graphene with monovacancy sites vary for different metal atoms, the diffusion barrier of a metal atom on defective graphene is always considerably higher than that on pristine graphene.[40] This conclusion agrees with the experimental results. For example, by combining *in situ* transmission electron microscopy, electron tomography, and molecular dynamics calculations, Moldovan and co-workers[41] found that Pt nanoparticles not only preferentially resided at the topographic defects of graphene (*e.g.*, steps and edges), but also diffused and coalesced along these defects after annealing at 700 °C.

In contrast to graphene, graphene oxide has a large number of oxygen-containing functional groups and topological defects.[42] These oxygen functional groups and topological defects can serve as more favorable anchoring centers and nucleation sites for the active species or the precursors.[43] Therefore, graphene oxide and its derivatives, rather than pristine graphene, have been used to prepare graphene-supported catalysts. The advantages of using graphene oxide as a support or precursor can be summarized as follows: (1) graphene oxide is cheaper and more readily available;[44] (2) the amphiphilic nature and excellent dispersibility of graphene oxide in both aqueous and organic solvents[31] render the surface more accessible to different precursors that can subsequently enhance the accessibility of the supported catalytically active species; (3) the binding energy of the oxygen-doped surface of graphene oxide toward metal atoms is significantly higher than that of pristine graphene[45] that subsequently increases the stability of the supported nanoparticles and their resistance to sintering. Moreover, the associated charge

transfer may significantly lower the reaction barrier without the need of introducing defects or strain;[46] (4) the covalent immobilization of catalytically active organic species or enzymes can be easily achieved by surface functionalization;[47] and (5) the redox reaction between graphene oxide and many metal ions may lead to spontaneous deposition of the metal nanoparticles on the basal plane of graphene.[48]

However, as mentioned in the Introduction section, the presence of functional groups and structural defects in graphene oxide will significantly reduce the electron mobility of pristine graphene that will subsequent affect electron transfer with the catalytically active species. Consequently, pristine graphene-, graphene oxide-, and r-GO-supported catalysts may show significant differences in catalytic performance, especially for supported electrocatalysts. For the supported noble metal electrocatalysts, a crucial role of the support is to provide a network with high electron conductance to minimize ohmic losses associated with electron transport. Therefore, using graphene supports with low defect density (such as solvent-exfoliated graphene[49]) and high electrical conductivity is more desirable for electrocatalysis. For example, Huang and Wang[50] demonstrated that Pd nanoparticles supported on low-defect graphene (LDG) sheets (prepared by a soft chemical method) showed an electrochemically active surface area that was twice as large as that on r-GO. LDG not only provided a large surface area, but also preserved the excellent electrical conductivity of pristine graphene for the electrocatalytic reactions.
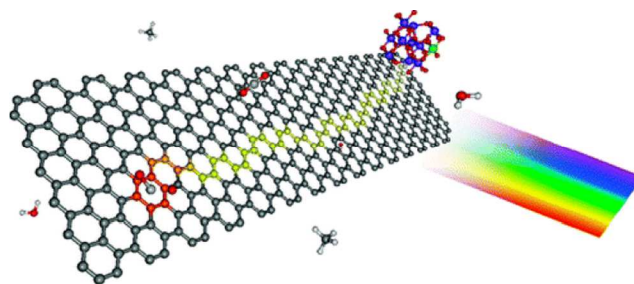

Fig. 2 Proposed photocatalytic mechanism for graphene–TiO_2 nanocomposites. The color code for the atoms is as follows: carbon (gray), hydrogen (white), oxygen (red), and titanium (blue). Upon illumination, the photo-excited electron is injected into the graphene nanoplatelet, leaving behind a TiO_2-confined hole (green). Because of the lower density of defects in solvent-exfoliated graphene, electrons are able to diffuse farther (depicted as the yellow pathway), thus providing a larger surface area for the adsorption of CO_2. Reproduced with permission from ref. 51. Copyright 2011, American Chemical Society.

A profound influence of defects on the catalytic performance was also observed with graphene-supported semiconductor photocatalysts. Despite many studies that suggest the positive influences of graphene and its derivatives on such types of photocatalysts, varied results involving different graphene supports have been observed in the photocatalytic degradation of pollutants, photocatalytic hydrogen generation, and photocatalytic disinfection.[27] It is expected that the photo-generated electrons in such graphene-supported semiconductor photocatalysts will move toward the graphene support, leaving behind the holes in the supported semiconductor particles.[51, 52] Thus, the graphene support acts as an electron acceptor to enhance separation between the photogenerated electron and

holes, thereby suppressing their recombination, and consequently enhancing the photocatalytic efficiency. Therefore, using graphene supports, prepared by different methods, featuring different conductivities significantly influences the final photocatalytic efficiency. For example, Hersam and co-workers[51] found that TiO_2 (P25) supported on solvent-exfoliated graphene (0.27 wt.% P25) exhibited higher photoreductive activity than pure P25 by 4.5× and 7.2× under ultraviolet and visible illumination, respectively. In comparison, the counterpart supported on r-GO showed no improvement under ultraviolet illumination, but a 2.3-fold enhancement was observed under visible illumination. The authors attributed the difference to the superior electrical mobility of the solvent-exfoliated graphene that contained fewer defects. In this photocatalytic system, graphene not only facilitates the dispersion of the semiconductor nanoparticles to prevents their agglomeration, but also reduced the electron–hole recombination rate of the supported TiO_2 by acting as an acceptor of photo-generated electrons (**Fig. 2**).

2.2. Influence of mass transfer

Apart from the intrinsic chemical activity, selectivity, and stability, the practical performance of a supported catalyst is also subject to physical limitation.[53] For conventional supported catalysts with a porous structure, the reaction only occurs when the reactant molecules come in contact with the supported active sites, which are usually located inside the pores. Typically, seven consecutive steps are involved in a classical heterogeneous catalytic reaction,[33] *i.e.*, (1) diffusion of the reactants from the bulk phase to the external surface of the catalyst (external diffusion); (2) diffusion of the reactants inside the pores to the immediate vicinity of the active sites (internal diffusion); (3) adsorption of the reactants onto the inner catalytic surface; (4) reaction at specific active sites; (5) desorption of the products from the inner surface; (6) diffusion of the products from the interior of the catalyst to its external surface (internal diffusion); and (7) diffusion of the products from its external surface to the bulk fluid (external diffusion).

Consequently, the observed reaction rate and selectivity of the targeted product also rely on the physical mass transfer/diffusion steps involved.[53] Many heterogeneous catalytic reactions are diffusion-controlled, especially for reactions in the liquid phase where the diffusion coefficient is much smaller than it is in the gas phase. The latter fact may partly explain the improved catalytic performance of graphene or graphene oxide-supported catalysts observed in many liquid-phase reactions. It is expected that the 2D structure with its large surface area and interesting surface chemistry not only affords high loading and stronger interactions with the targeted species, but also promotes mass transfer during the reaction.

For example, despite the variation of catalytic performances that was observed in samples prepared by different methods, graphene- and graphite oxide-supported Pd catalysts showed superior catalytic performance in organic synthetic reactons (such as the Suzuki–Miyaura cross-coupling reactions) than relative to conventional Pd/C catalysts.[54-64] Mulhaupt and co-workers[54] reported a remarkable turnover frequency (TOF) of 39,000 h^{-1} for a graphite oxide-supported Pd catalyst in the Suzuki–Miyaura reaction that is significantly higher than that achieved by a commercial Pd/C catalyst. A later study by Gupton and co-

workers reported an even higher TOF of 108,000 h^{-1} for a r-GO-supported Pd catalyst that was prepared by microwave-assisted chemical reduction of a palladium salt and graphite oxide.[56] Unprecedented TOFs of 230,000 and 237,000 h^{-1} have been reported for Pd on single layer graphene oxide or r-GO by different research groups.[57, 64]

As mass transfer resistance becomes less prominent or even negligible, supported bimetallic catalysts with higher catalytic activity become more attractive because the addition of a second metal can alter the electronic properties of the nanoparticle and will usually has a positive effect on the intrinsic chemical activity of the catalyst.[65-69] A series of graphene- and graphene oxide-supported bimetallic nanocatalysts in the forms of alloys, core–shell structures and other morphologies and various compositions were prepared and showed extraordinary activity in catalytic dehydrogenation, coupling reactions, reduction, and oxidation.[70-80] Besides, controlling the mass transfer processes to the highly active bimetallic nanocatalysts is an interesting strategy for adjusting their catalytic performance. For example, Fan and co-workers[81] developed a graphene-based smart catalytic system that consisted of graphene-supported Au@Pt bimetallic nanocatalysts and a thermally-responsive polymer. The authors showed that the catalytic reaction could be readily switched on or off by changing the diffusion limitation in different temperature windows.
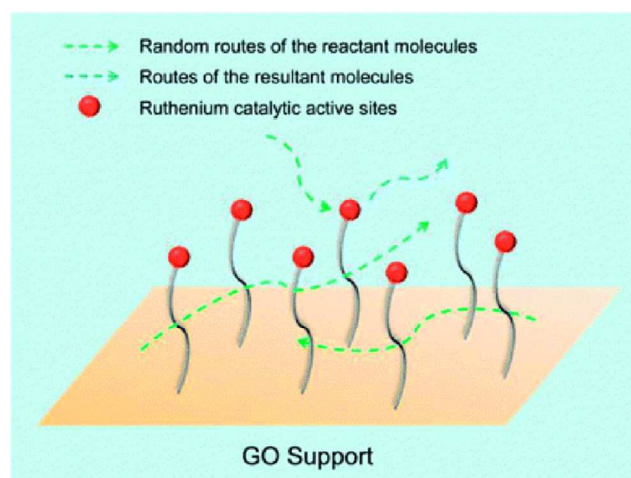

Fig. 3 Illustration for the mass transfer phenomenon in liquid phase. (The Reproduced permission from ref. 90. Copyright 2013, Royal Society of Chemistry).

Graphene-supported organic and organometallic catalysts have also attracted increasing attention over the past several years because such catalysts on conventional supports often display lower activity than their unsupported analogues. Diffusion effects are known to contribute to this problem.[82] Fan and co-workers demonstrated that sulfonated graphene could be used as a water-tolerant solid acid for the catalytic hydrolysis of ethyl acetate, and achieved a comparable activity to that of homogeneous sulfuric acid.[83] The excellent catalytic properties were attributed to the high acid density of the $-SO_3H$ anchor groups (1.55–2.0 mmol g^{-1}) and the crumpling feature of the sample that facilitated mass transfer of both the reactants and products. Similar results were obtained by other groups using sulfonated graphene prepared by hydrothermal sulfonation.[84] Amino-functionalized graphene/graphene oxide[85, 86] as well as the acid and base

bifunctional graphene/graphene oxide[87, 88] were examined as environmentally friendly catalysts for the hydrolysis of ethyl acetate, the nitrostyrene forming reaction, and the deacetalization–nitroaldol reaction. Interestingly, transition metal complexes immobilized on graphene oxide showed significantly enhanced catalytic activity when compared with equivalent homogeneous analogues.[89-91] Considering that transition metal complexes can form inactive dimers or aggregates in homogeneous solution,[82] the unusual enhanced activity of the immobilized transition metal complexes may be explained by a site-isolation effect, as well as by the access/release of the reactant and product to/from the catalytic sites in the pseudo-homogeneous system with limited mass transfer resistance (**Fig. 3**).
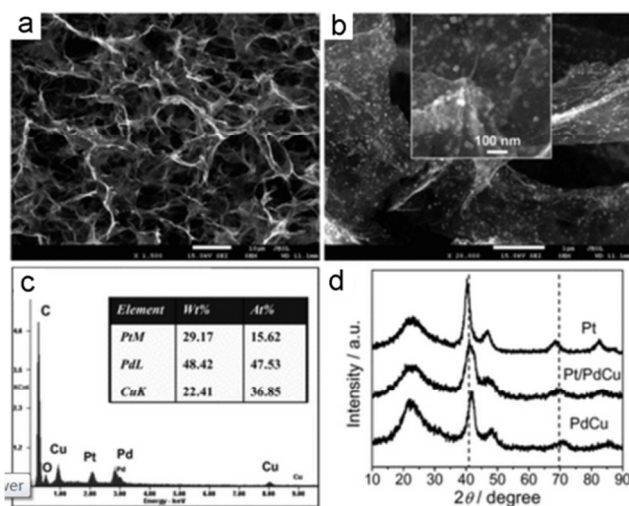

Fig. 4 (a,b) Field-emission scanning electron microscopy images of Pt/PdCu on 3D graphene frameworks (3DGF), (c) corresponding energy-dispersive X-ray spectroscopy pattern, and (d) X-ray diffraction patterns of Pt, PdCu, and Pt/PdCu on 3DGF. The inset in (b) is a high magnification view of cubic Pt/PdCu on graphene sheets. Reproduced with permission from ref. 95. Copyright 2012, WILEY-VCH.

In contrast to the suspended graphene or graphene oxide nanosheets used in the reactions above, three-dimensional (3D) graphene frameworks/networks[92] may be a better choice of support for use in solid-state catalysts. The 3D structure not only provides high specific surface areas and high strength endurance for catalyst loading, but also facilitates the rapid mass transfer of the reactants, products and electrolyte. Wang and co-workers[93] prepared a series of 3D graphene-supported noble metal nanocrystals through macro-assembly of graphene oxide. The authors demonstrated that the supported Pd could be used as a fixed-bed catalyst in the Heck reaction, achieving 100% selectivity and 100% conversion. Aside from applications in organic synthesis, 3D graphene is highly desirable for use as a graphene-based catalyst electrode, as mass transfer has profound effects on the catalytic performance of the electrode.[12] It is well known that catalyst electrodes must provide an electrical conductive path for the transport of electrons and an ionically conductive path for the transport of protons, as well as channels for the transport of reactants and products. However, in solid-state electrodes, graphene sheets tend to stack on each other in a parallel arrangement during electrode assembly because of the

strong van der Waals forces and π–π stacking interactions. Although the supported nanoparticles can act as spacers,[94] film-like architectures with low accessible surface area and high mass transfer resistance are often observed with the graphene-based electrodes. A reduced catalytic performance of a graphene-based electrode may be expected owing to the restacking phenomenon. Therefore, to provide maximum accessibility of the active species to the catalyst and to ensure efficient mass transfer of the reactants and/or products, Qu and co-workers[95] developed 3D graphene framework-supported ternary Pt/PdCu nanoboxes for anodic electrocatalysis. The authors reported more than 6-fold improvement in activity per unit mass of Pt relative to the activity achieved by a commercial Pt/C catalyst (**Fig. 4**). In a study of Fe_3O_4 nanoparticles for oxygen reduction reaction (ORR), Müllen and co-workers[96] demonstrated that 3D N-doped graphene-supported Fe_3O_4 nanoparticles electrocatalyst had obviously enhanced ORR activity when compared with the other counterparts of similar compositions. The authors believed the enhanced performances could be partly attributed to the positive effect of macropores on the diffusion rate of the electrolyte to the exposed active sites. The performance of many graphene-based biosensors is also reliant on mass transfer processes, as exemplified. In a study on 3D graphene-supported CuO biosensor for ascorbic acid detection, Huang and co-workers[97] showed that the anodic peak current was proportional to the square root of the scan rate. This result suggested that the redox reaction was controlled by mass transfer processes,[98] and highlighted the advantages of the 3D architecture in providing an ideal morphology for mass transfer.

3. Catalytic properties of graphene

In addition to its use as a catalyst support, graphene and its derivatives find applications as metal-free catalysts. The advantages of these catalysts include their lack of sensitivity to moisture and oxygen, potential low cost, and low toxicity when compared with metal catalysts. More specifically, graphene-based carbocatalysts have shown great promise for potential applications in various reactions. Their catalytic activity is attributed to the presence of edges/defects, functional groups, or doping structures that not only alter the chemical and physical properties of pristine graphene, but also completely change their roles in many heterogeneous catalytic reactions. In particular, oxygen- and nitrogen-containing functionalities, which can be incorporated into graphene by diverse methods, play important roles in this intrinsic catalytic activity. In this section, the origin of the intrinsic catalytic activity of graphene is discussed.

3.1. Intrinsic catalytic activity originating from oxide functional groups and edges/defects

In contrast to pristine graphene that features inert activity, graphene oxide and its reduced counterpart, r-GO, have been proven to be promising catalysts for many catalytic reactions, especially in organic synthesis. However, the determination of the complete structure of graphene oxide and r-GO has remained elusive because of their non-stoichiometric nature and complex changes in structure. Herein, we briefly describe some key features that are necessary to understand the origin of the catalytic activity of graphene oxide and r-GO.

Graphene oxide can be regarded as a 2D network consisting of variable concentrations of sp^2 and sp^3 carbon, with abundant hydroxyl and epoxy functional groups on the basal plane. Additionally, high-resolution ^{13}C NMR spectroscopy has revealed the presence of lactol, ester carbonyl, and ketone functional groups at the edges or defects of graphene oxide.[99] A complete structure of graphene oxide constituting five- and six-membered lactol rings decorating the edges as well as esters of tertiary alcohols on the surface has been proposed (**Fig. 5**).[100] Although most the hydroxyl and epoxy functional groups can be removed after the reduction of graphene oxide, the holes, Stone-Wales and other defects are usually observed within the basal plane. Besides, highly stable carbonyl and ether groups are also remained at the edges/defects.[101] Additionally, trace amounts of other heteroatom-containing functionalities, such as sulfate groups, may be present, as introduced upon adsorption during the preparation of graphite oxide by the Hummers method.[102]
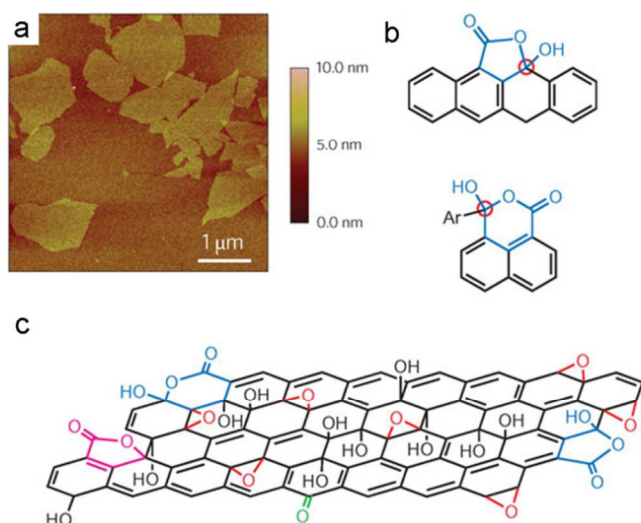

Fig. 5 Atomic force microscopy image and structural models of graphene oxide: (a) atomic force microscopy image of graphene oxide sheets on a silicon substrate; (b) structure consisting of five- and six-membered lactol rings. The carbons circled in red are those that generate ^{13}C NMR signals at 101 ppm; (c) alternative structural model of graphene oxide, taking into account five- and six-membered lactol rings (blue), ester of a tertiary alcohol (pink), hydroxyl (black), epoxy (red), and ketone (green) functionalities. Reproduced with permission from ref. 100. Copyright 2009, Nature Publishing Group.

These heteroatom-containing functionalities, edges, topological defects, as well as subsequent changes in the electronic properties contribute to the intrinsic catalytic activity of graphene oxide and r-GO. However, the nature of the catalytically active sites in specific reactions remains under debate. Bielawski and co-workers[103, 104] reported that graphene oxide could be used as a carbocatalyst for the oxidation of alcohols and alkenes, the hydration of alkynes, as well as for the polymerization of various olefins. In the oxidation reactions, the authors showed that the yield of the final products significantly decreased when the oxidation reaction was performed under an atmosphere of nitrogen, suggesting the catalytic role of graphene oxide. A subsequent density functional theory (DFT) calculation study revealed that the reaction occurred *via* the transfer of hydrogen atoms from the organic molecule to the epoxide groups on the basal plane of graphene oxide, followed by ring-opening

reactions and dehydration that resulted in the formation of partially reduced graphene oxide. However, the partially reduced catalyst could be regenerated by molecular oxygen that allowed for catalyst recycling.[105] In another DFT study on the oxidative dehydrogenation of propane to propene over graphene oxide, Tang and Cao[106] showed that the epoxy groups on the graphene oxide surface provided active sites for the C–H bond activation, and the presence of hydroxyl groups around the epoxide active sites remarkably enhanced the C–H bond activation of propane (**Fig. 6**). However, the widespread application of graphene oxide in these oxidative reactions is still limited by high catalyst loading requirements.
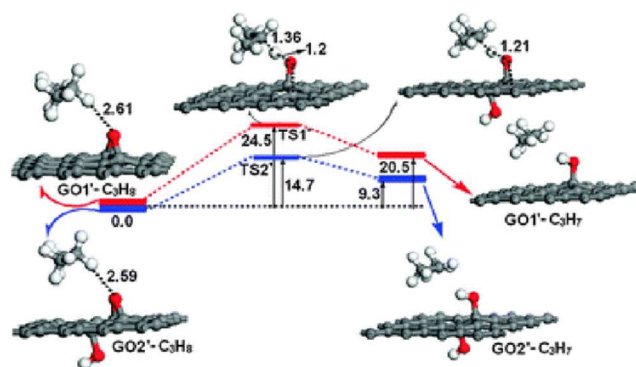

Fig. 6 Relative energy profiles for the first H abstraction from CH_2 of propane on graphene oxide GO1' and GO2'. The red and blue lines represent the pathways adopted by two different GO structures including one epoxide group (GO1') and one added neighboring OH at the opposite side with respect to other oxygen groups on GO1' (GO2'), respectively. All energies (kcal mol^{-1}) are relative to propane adsorbed onto GO, and the optimized configurations (distances in Å) of the initial, transition, and final states are shown. Reproduced with permission from ref. 106. Copyright 2012, Royal Society of Chemistry.

An electron transfer mechanism has been proposed for the intrinsic peroxidase-like activity of graphene oxide and its derivatives.[107-109] Qu and co-workers[107] reported that carboxyl-modified graphene oxide showed intrinsic peroxidase-like activity and catalyzed the reaction of peroxidase by H_2O_2. The authors believed that the catalytic effect was related to the electronic structures of graphene oxide and its interactions with H_2O_2, *i.e.*, the electron transfer occurred from the top of the valence band of graphene oxide to the lowest unoccupied molecular orbital (LUMO) of H_2O_2.[110] In the luminol-H_2O_2 system, Huang and co-workers[109] demonstrated the role of graphene oxide in increasing the rate of the electron transfer processes. By using chemiluminescence spectroscopy, UV−visible absorption spectroscopy, and electron spin resonance spectroscopy, the authors found that the $^1O_2$-induced chemiluminescence was greatly enhanced upon introduction of graphene oxide in the system.

In contrast, in the r-GO system, the remaining functional groups (carboxylic acid groups, in particular) and unsaturated carbon atoms at the edges and defects play crucial roles in the intrinsic catalytic activity. For example, Bao and co-workers[111] demonstrated that r-GO could be used as a catalyst for the reduction of nitrobenzene at room temperature. The authors proposed that the unsaturated carbon atoms at the edges and defects may be catalytically active centers for nitrobenzene; DFT calculations suggested that the carbon atoms at the zigzag edges
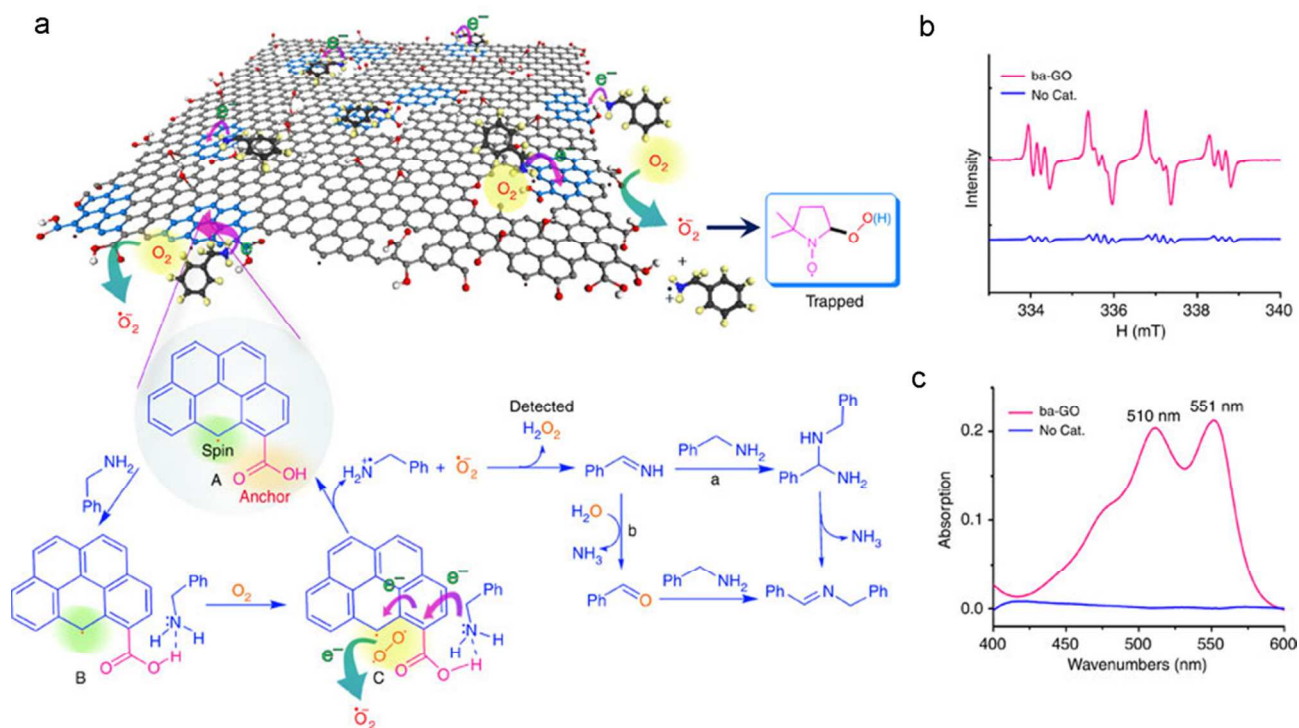
Fig. 7 Mechanism of r-GO-catalyzed oxidative coupling of primary amines. (a) Schematic representation of the oxidation mechanism. (b) DMPO spin-trapped electron paramagnetic resonance spectra in the presence and absence of catalyst; in the presence of ba-GO catalyst and O_2, the spin signals corresponding to DMPO–OO(H) are more intense and predominant. (c) UV–visible absorption spectra of the reaction system in the presence and absence of catalyst after adding DPD. Reproduced with permission from ref. 113. Copyright 2012, Nature Publishing Group.

of the graphene sheet could interact with both terminal oxygen atoms of nitrobenzene. This conclusion was supported by another study (by the same authors) on the electrocatalytic activity of different sized graphene sheet in the ORR.[112]

Subsequently, a detailed study by Loh and co-workers[113] on the catalytic activity of r-GO toward the oxidative coupling of amines revealed the synergistic effect of carboxylic acid groups and unpaired electrons at the edge defects. The authors observed that regeneration of the carboxyl groups on r-GO after a neutralization treatment was accompanied by a remarkable recovery in the catalytic activity, whereas quenching of the localized spins generated at the edges or defects was associated with a decrease in the catalytic activity from 89% to 30%. These results provided strong evidences that the carboxylic acid groups and the edges/defects of r-GO play vital roles in catalytic reactions. Therefore, an interesting mechanism of the oxidative coupling of primary amines catalyzed by r-GO was proposed (**Fig. 7**). Additionally, the ketonic (C=O) groups at the edges/defects of r-GO that are rich in electrons may coordinate a redox process.[114]

It should be noted that other heteroatom-containing functionalities, such as sulfate groups, may also play a crucial role in the catalytic performance of graphene oxide. For example, Garcia and co-workers[115] showed that graphene oxide could be used as a recyclable acid catalyst for the ring opening of epoxides at room temperature. The main acid sites may be attributed to both the carbonyl groups and minute amounts of hydrogen sulfate groups that were introduced during the preparation of the graphite

oxide precursor. A similar study on the catalytic acetalization of aldehydes showed that the sulfur content on graphene oxide decreased from 1.0 to 0.6 wt.% following washing with methanol, resulting in a significant decrease in the catalytic activity.[116] These results suggested that the sulfate groups spontaneously introduced during Hummers oxidation may be the main acid sites that are responsible for many acid catalytic reactions by graphene oxide.

3.2. Intrinsic catalytic activity originating from doping

Doping graphene with heteroatoms, such as N, B, P, I and S, has proved to be an effective method to modify the electron-donor properties and to endow graphene intrinsic catalytic activity.[117-139] N-doped graphene and its dual doping counterparts, in particular, have been demonstrated to be promising metal-free catalysts for oxygen reduction reaction (ORR). Despite numerous studies that have been performed, the catalytic active sites and the mechanisms involved remain controversial. Pyridinic-N (or pyrrolic-N) and graphitic-N are usually considered to be responsible for the ORR activity of N-doped graphene. Where pyridinic-N (or pyrrolic-N) at the edges or defects is the nitrogen that contributes one p-electron to the aromatic π-system, and graphitic-N refers to the N atoms replacing the C atoms inside the graphene basal plane (**Fig. 8d**).[117] However, either pyridinic-N or graphitic-N should be responsible for the enhanced catalytic activity of N-doped graphene is still under debate.
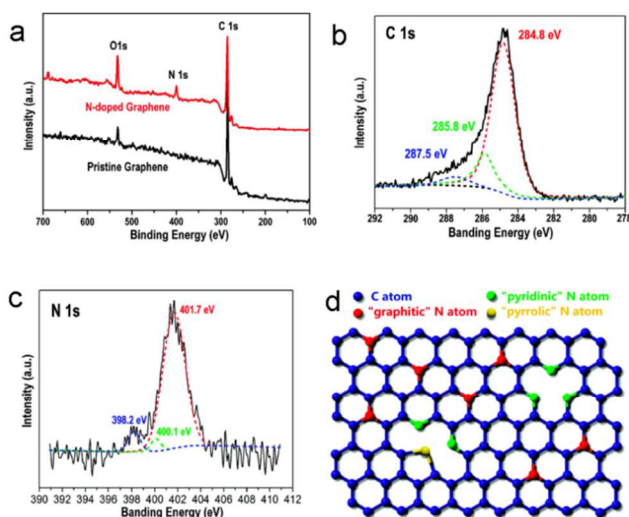
Fig. 8 (a) X-ray photoelectron spectroscopy patterns of pristine graphene and N-doped graphene. X-ray photoelectron spectroscopy (b) C 1s pattern and (c) N 1s pattern of N-doped graphene. The C 1s peak can be split into three Lorentzian peaks at 284.8, 285.8, and 287.5 eV, which are indicated by the red, green, and blue dashed lines, respectively. The N 1s peak can be split into three Lorentzian peaks at 401.7, 400.1, and 398.2 eV, which are indicated by the red, green, and blue dashed lines, respectively. (d) Schematic representation of N-doped graphene. The blue, red, green, and yellow spheres represent C, graphitic-N, pyridinic-N, and pyrrolic-N atoms in N-doped graphene, respectively. Reproduced with permission from ref. 117. Copyright 2009, American Chemical Society.

It is known that the nitrogen bonding configurations, rather than the nitrogen content, is the key factor for the electrocatalytic performance of N-doped graphene towards the ORR.[122, 127] For example, Xia and co-workers[122] prepared N-doped graphene *via* thermal annealing of graphite oxide with melamine. The atomic percentage of nitrogen in the doped graphene samples could be adjusted to up to 10%. The authors showed that the nitrogen content in N-doped graphene did not significantly influence the electrocatalytic activity of N-doped graphene towards the ORR.

Pyridinic-N sites have been widely regarded as catalytically active sites for N-doped carbon materials owing to the delocalization of the p electron from pyridinic-N that facilitates the reductive O_2 adsorption. By using graphene oxide as a precursor, Müllen and co-workers[123] observed that the content of pyridinic-N and the electrical conductivity are the two key factors for achieving high-performance N-doped graphene for the ORR. When the content of graphitic-N was reduced while that of pyridinic-N was kept constant by increasing the pyrolysis temperature from 800 to 1000 °C, they observed an obvious decrease in the ORR catalytic activity was observed. A recent study[138] using synchrotron-based X-ray photoelectron spectroscopy showed that oxygen reduction intermediate, OH_{ads}, which is expected to chemically attach to the active sites, remained on the carbon atoms close to the pyridinic-N after the ORR. This result suggested that pyridinic-N played an important role in the ORR process and that the nearby carbon atoms are the main active sites, as consistent with the theoretical studies.[125, 133] DFT calculations revealed that identification of the catalytically active sites on N-graphene was mainly governed by the spin density distribution. The substituted nitrogen atoms that introduce unpaired electrons into the graphene will change the atomic charge distribution on graphene. Therefore, the carbon atoms neighboring pyridinic nitrogen have the highest spin density (**Fig. 9**) and hence are the electrocatalytically active catalytic sites.[125]
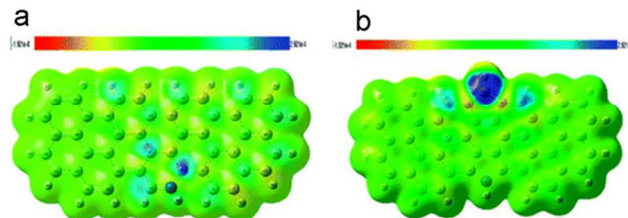

Fig. 9 Spin density distribution on N-graphene with (a) a pyridine structure ($C_{45}NH_{20}$) and (b) a pyrrole structure ($C_{45}NH_{18}$) , respectively. Spin density distributes on the electron density isovalue plane; the most negative value is indicated by the red region in the scale bar, whereas the most positive value is indicated by the blue region in the scale bar. Reproduced with permission from ref. 125. Copyright 2011, American Chemical Society.

However, when pure pyridinic-N doped graphene that was prepared by the chemical vapor deposition was used, the as-prepared N-doped graphene did not show remarkable ORR catalytic ability as previously reported.[120] In another study, the same group found that annealing graphene oxide with ammonia preferentially formed graphitic-N and pyridinic-N centers, whereas annealing of polyaniline/r-GO and polypyrrole/r-GO generally produced pyridinic and pyrrolic-N moieties, respectively. Additionally, they found that the electrocatalytic activity of the catalyst was dependent on the graphitic-N content, whereas varying the content of pyridinic-N improved the onset potential for ORR.

Thus, both pyridinic and graphitic nitrogen may contribute to the catalytic performance, while assuming different roles. In a study on the catalytic activity of graphite nitride, Wang and co-workers[140] reported that the N atoms, especially the graphitic-N atoms in the carbon lattice, could facilitate electron transfer from the carbon electronic bands to the antibonding orbitals of O_2. Additionally, Zhang and Xia[125] reported that the graphitic-type doping showed ORR activity in both dissociative and associative paths. Jung and co-workers[119] reported an inter-conversion event between the graphitic and pyridinic sites within a catalytic cycle. Based on their calculations, the outermost graphitic nitrogen site in particular gave the most desirable characteristics for improved ORR activity, and hence acted as the active site. But the latter graphitic nitrogen would become pyridinic-like in the subsequent electron and proton transfer reaction *via* ring-opening of a cyclic C–N bond. However, in a recent study by Woo and co-workers,[135] based on DFT calculations (considering entropic contributions and solvation effects), no thermodynamically suitable sites for O_2 binding near the N-doped carbon sites were identified except for the graphitic-N sites specifically positioned at the edge of graphene sheet. The authors suggested that oxygen adsorption was not necessary for ORR of N-doped graphene, and the first electron was transferred to O_2 molecules at the outer Helmholtz plane (ET-OHP) over a long distance (**Fig. 10**). The ET-OHP mechanism may resolve the conundrum of finding thermodynamically unstable O_2 binding sites and allow the participation of basal graphene N-doped sites for the activation of oxygen.

Fig. 10 Starting from solvated O_2 molecules, the pathway is divided into ET-OHP and ET-IHP processes. For ET-OHP, O_2 adsorption is not necessary ($\Delta G_{ads}^{O_2} > 0$), and the rate of ET is strongly affected by the ionic strength of the electrolyte; for ET-IHP, it is important to find good O_2 adsorption sites ($\Delta G_{ads}^{O_2} < 0$), and the electron can be injected into the O_2 π^* orbital through orbital–orbital interaction on the femtosecond timescale. From the DFT energetics, only the graphitic-N sites at the edge of the graphene sheet can adsorb O_2 and enable the ET-IHP mechanism only at these sites; however, this mechanism cannot be fully reconciled with the observed ORR kinetics. The ET-OHP process will therefore predominantly occur on the basal plane where O_2 adsorption is unfavorable. After formation of •OOH at the end of the ET-OHP process, •OOH immediately adsorbs onto the N-doped graphene surface ($\Delta G_{ads}^{•OOH} < 0$); this allows further stable reduction steps that generate two water molecules (the four electron pathway). Reproduced with permission from ref. 135. Copyright 2014, American Chemical Society.

In addition to N-doped graphene, other heteroatom-doped graphenes, and co-doped graphene in particular have generated increasing interest.[128, 130, 131, 134, 137] For example, Qiao and co-workers[128] found that the S- and N- co-doped graphene catalysts had significantly better ORR performance than graphene catalysts doped solely with S or N atoms. A calculation study revealed that the maximum spin density substantially increased to 0.43 when S and N were simultaneously incorporated into graphene to form co-doped graphene, resulting in significantly improved ORR activity. Dai and co-workers[141] prepared a B- and N-co-doped graphene catalyst by thermally annealing graphene oxide in the presence of boric acid and ammonia, and the resultant co-doped graphene showed superior electrocatalytic activity over a commercial Pt/C electrocatalyst. First-principles calculations revealed that the N and B-co-doping could result in a smaller energy gap when compared with that in pure graphene, thereby leading to improved catalytic activity. However, only moderate doping could enhance the electrocatalytic activity of graphene towards the ORR. Co-doping with excessive amounts of B and N could result in significantly decreased catalytic activity. Qiao and co-workers[134] also observed a synergistic coupling effect between N and B co-dopants. The authors reported that the 2p orbital of the C atom located between the N and B dopants was first polarized by N, which was then able to donate extra electrons to an adjacent B atom. Consequently, the electron occupancy of the 2p orbital of the "activated" B atom increased, thereby facilitating adsorption and bonding with HO_2. Thus, the activated B atom served as an active site to enhance the ORR activity. Moreover, a recent DFT simulations study by Kiefer and co-workers[137] identified graphitic BN_3 motifs as active sites for complete O_2 electroreduction using B- and N-co-doped graphene electrocatalyst. The studies predicted that an enhancement in catalytic activity and selectivity could be achieved by increasing the concentration of graphitic BN_3 motifs.

4. Conclusions and outlook

Because of the rapid expansion in the number of studies related to the applications of graphene in heterogeneous catalysis, rather than attempting to summarize all the progress achieved to date, we discuss the role of graphene and its derivatives as catalyst supports, with particular emphasis on the influence of defects and functional groups on their interaction with catalytic phases, as well as the advantages of structures in the mass transfer process. Additionally, we provide a comprehensive summary on the contribution of edges/defects, functional groups, and doping structures to the intrinsic catalytic properties of graphene-based catalysts.

Although substantial progress has been made during the past several years, research toward the applications of graphene in heterogeneous catalysis is still at its early stages. Many important challenges must be addressed before practical applications are fully developed. First, despite the fact that enhanced catalytic performances was observed in most graphene-based supported catalysts studied to date, a systematical comparison with commercial catalysts remains necessary. In particular, the catalyst should at least show comparable stability and performance under the required reaction conditions for long periods of time. Most experimental studies on graphene-supported catalysts have focused on the preparation, characterization, and quantification of their catalytic activity in specific reactions. In contrast, studies on the fundamental principles and parameters that influence the catalyst performance are rare. For example, mass transfer has been shown to have a prominent influence on the catalytic performance of graphene-supported catalysts, but detailed models describing the transport of reactants and products to and from the active sites have yet to be determined. As for graphene-based catalysts, the intrinsic catalytic properties give graphene and its derivatives great promise for potential applications as metal-free catalysts in diverse reactions. Unfortunately, identifying the actual active sites on these catalysts is still a great challenge because of their structural complexity that originates from different types of functionalities, sites, edges and defects. To, shed some light on this problem, further studies that combine *in situ* characterization methods with theoretical calculations are necessary.

Despite these remaining challenges, the future of graphene-based supports and catalysts is exciting, considering that carbon-based supports and catalysts have been used in numerous reactions of industrial interest.[3] Additionally, it is apparent from the literature coverage in this review that high-quality graphene is not necessary for application in heterogeneous catalysis, and thus may reduce the gap between basic scientific research and industrial development in terms of economical and technical factors.

Acknowledgements

Notes and references

ᵃ School of Chemical Engineering and Technology, Tianjin University, Tianjin 300072, China. E-mail: xiaobinfan@tju.edu.cn Fax: +86-22-27890090

ᵇ Collaborative Innovation Center of Chemical Science and Engineering (Tianjin)

ᶜ State Key Laboratory of Chemical Engineering, Tianjin University

1. P. o. N. D. i. C. S. a. Technology, *Catalysis Looks to the Future*, 1992, National Academy Press, Washington D.C., 1.
2. F. Rodriguez-Reinoso, *Carbon*, 1998, **36**, 159-175.
3. L. R. Radovic and F. Rodriguez-Reinoso, in *Chemistry and Physics of Carbon, Vol 25*, ed. P. A. Thrower, 1997, vol. 25, pp. 243-358.
4. *Nature Nanotechnol.*, 2010, **5**, 755-755.
5. K. S. Novoselov, A. K. Geim, S. V. Morozov, D. Jiang, Y. Zhang, S. V. Dubonos, I. V. Grigorieva and A. A. Firsov, *Science*, 2004, **306**, 666-669.
6. R. R. Nair, P. Blake, A. N. Grigorenko, K. S. Novoselov, T. J. Booth, T. Stauber, N. M. R. Peres and A. K. Geim, *Science*, 2008, **320**, 1308-1308.
7. A. A. Balandin, S. Ghosh, W. Z. Bao, I. Calizo, D. Teweldebrhan, F. Miao and C. N. Lau, *Nano Lett.*, 2008, **8**, 902-907.
8. C. Lee, X. D. Wei, J. W. Kysar and J. Hone, *Science*, 2008, **321**, 385-388.
9. C. N. R. Rao, A. K. Sood, K. S. Subrahmanyam and A. Govindaraj, *Angew. Chem. Int. Ed.*, 2009, **48**, 7752-7777.
10. M. J. Allen, V. C. Tung and R. B. Kaner, *Chem. Rev.*, 2010, **110**, 132-145.
11. P. Avouris, Z. H. Chen and V. Perebeinos, *Nat. Nanotech.*, 2007, **2**, 605-615.
12. D. A. C. Brownson, D. K. Kampouris and C. E. Banks, *Chem. Soc. Rev.*, 2012, **41**, 6944-6976.
13. D. Chen, L. H. Tang and J. H. Li, *Chem. Soc. Rev.*, 2010, **39**, 3157-3180.
14. Y. Chen, B. Zhang, G. Liu, X. D. Zhuang and E. T. Kang, *Chem. Soc. Rev.*, 2012, **41**, 4688-4707.
15. L. M. Dai, *Acc. Chem. Res.*, 2013, **46**, 31-42.
16. S. J. Guo and S. J. Dong, *Chem. Soc. Rev.*, 2011, **40**, 2644-2672.
17. X. Huang, X. Y. Qi, F. Boey and H. Zhang, *Chem. Soc. Rev.*, 2012, **41**, 666-686.
18. K. Kim, J. Y. Choi, T. Kim, S. H. Cho and H. J. Chung, *Nature*, 2011, **479**, 338-344.
19. M. M. Liu, R. Z. Zhang and W. Chen, *Chem. Rev.*, 2014, **114**, 5117-5160.
20. M. Pumera, *Chem. Soc. Rev.*, 2010, **39**, 4146-4157.
21. S. Roth and H. J. Park, *Chem. Soc. Rev.*, 2010, **39**, 2477-2483.
22. F. Schwierz, *Nat. Nanotechnol.*, 2010, **5**, 487-496.
23. X. J. Wan, Y. Huang and Y. S. Chen, *Acc. Chem. Res.*, 2012, **45**, 598-607.
24. D. C. Wei, B. Wu, Y. L. Guo, G. Yu and Y. Q. Liu, *Acc. Chem. Res.*, 2013, **46**, 106-115.
25. K. Yang, L. Z. Feng, X. Z. Shi and Z. Liu, *Chem. Soc. Rev.*, 2013, **42**, 530-547.
26. X. K. Kong, C. L. Chen and Q. W. Chen, *Chem. Soc. Rev.*, 2014, **43**, 2841-2857.
27. Q. J. Xiang, J. G. Yu and M. Jaroniec, *Chem. Soc. Rev.*, 2012, **41**, 782-796.
28. H. Wang and H. Dai, *Chem. Soc. Rev.*, 2013, **42**, 3088-3113.
29. H. A. Becerril, J. Mao, Z. Liu, R. M. Stoltenberg, Z. Bao and Y. Chen, *Acs Nano*, 2008, **2**, 463-470.
30. D. Li, M. B. Muller, S. Gilje, R. B. Kaner and G. G. Wallace, *Nat. Nanotechnol.*, 2008, **3**, 101-105.
31. J. I. Paredes, S. Villar-Rodil, A. Martinez-Alonso and J. M. D. Tascon, *Langmuir*, 2008, **24**, 10560-10564.
32. S. Navalon, A. Dhakshinamoorthy, M. Alvaro and H. Garcia, *Chem. Rev.*, 2014, **114**, 6179-6212.
33. G. Ertl, H. Knözinger and J. Weitkamp, *Handbook of Heterogeneous Catalysis*, 2008.
34. M. A. Zhou, A. H. Zhang, Z. X. Dai, Y. P. Feng and C. Zhang, *J. Phys. Chem. C*, 2010, **114**, 16541-16546.
35. G. Kim, Y. Kawazoe and K. R. Lee, *J. Phys. Chem. Lett.*, 2012, **3**, 1989-1996.
36. H. T. Wang, Q. Feng, Y. C. Cheng, Y. B. Yao, Q. X. Wang, K. Li, U. Schwingenschogl, X. X. Zhang and W. Yang, *J. Phys. Chem. C*, 2013, **117**, 4632-4638.
37. G. Kim and S. H. Jhi, *Acs Nano*, 2011, **5**, 805-810.
38. D. H. Lim and J. Wilcox, *J. Phys. Chem. C*, 2011, **115**, 22742-22747.
39. I. Fampiou and A. Ramasubramaniam, *J. Phys. Chem. C*, 2012, **116**, 6543-6555.
40. Y. N. Tang, Z. X. Yang and X. Q. Dai, *J. Chem. Phys.*, 2011, **135**.
41. M. S. Moldovan, H. Bulou, Y. J. Dappe, I. Janowska, D. Begin, C. Pham-Huu and O. Ersen, *J. Phys. Chem. C*, 2012, **116**, 9274-9282.
42. D. Chen, H. B. Feng and J. H. Li, *Chem. Rev.*, 2012, **112**, 6027-6053.
43. P. Kundu, C. Nethravathi, P. A. Deshpande, M. Rajamathi, G. Madras and N. Ravishankar, *Chem. Mater.*, 2011, **23**, 2772-2780.
44. D. R. Dreyer, S. Park, C. W. Bielawski and R. S. Ruoff, *Chem. Soc. Rev.*, 2010, **39**, 228-240.
45. M. N. Groves, C. Malardier-Jugroot and M. Jugroot, *J. Phys. Chem. C*, 2012, **116**, 10548-10556.
46. M. Yang, M. Zhou, A. H. Zhang and C. Zhang, *J. Phys. Chem. C*, 2012, **116**, 22336-22340.
47. V. Georgakilas, M. Otyepka, A. B. Bourlinos, V. Chandra, N. Kim, K. C. Kemp, P. Hobza, R. Zboril and K. S. Kim, *Chem. Rev.*, 2012, **112**, 6156-6214.
48. X. M. Chen, G. H. Wu, J. M. Chen, X. Chen, Z. X. Xie and X. R. Wang, *J. Am. Chem. Soc.*, 2011, **133**, 3693-3695.
49. J. N. Coleman, *Acc. Chem. Res.*, 2013, **46**, 14-22.
50. H. J. Huang and X. Wang, *J. Mater. Chem.*, 2012, **22**, 22533-22541.
51. Y. T. Liang, B. K. Vijayan, K. A. Gray and M. C. Hersam, *Nano Lett.*, 2011, **11**, 2865-2870.
52. I. V. Lightcap, T. H. Kosel and P. V. Kamat, *Nano Lett.*, 2010,

10, 577-583.

53.   R. Klaewkla, M. Arend and W. F. Hoelderich, *Mass Transfer - Advanced Aspects*, 2011, Chapter 29: A Review of Mass Transfer Controlling the Reaction Rate in Heterogeneous Catalytic Systems.

54.   G. M. Scheuermann, L. Rumi, P. Steurer, W. Bannwarth and R. Mulhaupt, *J. Am. Chem. Soc.*, 2009, **131**, 8262-8270.

55.   Y. Li, X. B. Fan, J. J. Qi, J. Y. Ji, S. L. Wang, G. L. Zhang and F. B. Zhang, *Nano Res.*, 2010, **3**, 429-437.

56.   A. R. Siamaki, A. E. S. Khder, V. Abdelsayed, M. S. El-Shall and B. F. Gupton, *J. Catal.*, 2011, **279**, 1-11.

57.   S. Moussa, A. R. Siamaki, B. F. Gupton and M. S. El-Shall, *ACS Catal.*, 2012, **2**, 145-154.

58.   Y. Nishina, J. Miyata, R. Kawai and K. Gotoh, *RSC Adv.*, 2012, **2**, 9380-9382.

59.   K. Qu, L. Wu, J. Ren and X. Qu, *Acs Appl. Mater. Inter.*, 2012, **4**, 5001-5009.

60.   S. Santra, P. K. Hota, R. Bhattacharyya, P. Bera, P. Ghosh and S. K. Mandal, *Acs Catal.* 2013, **3**, 2776-2789.

61.   N. Shang, C. Feng, H. Zhang, S. Gao, R. Tang, C. Wang and Z. Wang, *Catal. Commun.*, 2013, **40**, 111-115.

62.   L. Ma'mani, S. Miri, M. Mahdavi, S. Bahadorikhalili, E. Lotfi, A. Foroumadi and A. Shafiee, *Rsc Adv.*, 2014, **4**, 48613-48620.

63.   V. Sharavath and S. Ghosh, *Rsc Adv.*, 2014, **4**, 48322-48330.

64.   S.-i. Yamamoto, H. Kinoshita, H. Hashimoto and Y. Nishina, *Nanoscale*, 2014, **6**, 6501-6505.

65.   W. T. Yu, M. D. Porosoff and J. G. G. Chen, *Chem. Rev.*, 2012, **112**, 5780-5817.

66.   M. Sankar, N. Dimitratos, P. J. Miedziak, P. P. Wells, C. J. Kiely and G. J. Hutchings, *Chem. Soc. Rev.*, 2012, **41**, 8099-8139.

67.   Z. H. Wei, J. M. Sun, Y. Li, A. K. Datye and Y. Wang, *Chem. Soc.Rev.*, 2012, **41**, 7994-8008.

68.   F. Gao and D. W. Goodman, *Chem. Soc. Rev.*, 2012, **41**, 8009-8020.

69.   D. M. Alonso, S. G. Wettstein and J. A. Dumesic, *Chem. Soc. Rev.*, 2012, **41**, 8075-8098.

70.   H. Y. Chen, Y. Li, F. B. Zhang, G. L. Zhang and X. B. Fan, *J. Mater. Chem.*, 2011, **21**, 17658-17661.

71.   J. Wang, Y. L. Qin, X. Liu and X. B. Zhang, *J. Mater. Chem.*, 2012, **22**, 12468-12470.

72.   O. Metin, S. F. Ho, C. Alp, H. Can, M. N. Mankin, M. S. Gultekin, M. F. Chi and S. H. Sun, *Nano Res.*, 2013, **6**, 10-18.

73.   J. J. Qi, W. P. Lv, G. H. Zhang, Y. Li, G. L. Zhang, F. B. Zhang and X. B. Fan, *Nanoscale*, 2013, **5**, 6275-6279.

74.   J. M. Yan, Z. L. Wang, H. L. Wang and Q. Jiang, *J. Mater. Chem.*, 2012, **22**, 10990-10993.

75.   J. Chai, F. H. Li, Y. W. Hu, Q. X. Zhang, D. X. Han and L. Niu, *J. Mater. Chem.*, 2011, **21**, 17922-17929.

76.   T. Wu, J. K. Ma, X. R. Wang, Y. Liu, H. Xu, J. P. Gao, W. Wang, Y. Liu and J. Yan, *Nanotechnology*, 2013, **24**.

77.   R. Awasthi and R. N. Singh, *Carbon*, 2013, **51**, 282-289.

78.   X. M. Chen, Z. X. Cai, X. Chen and M. Oyama, *J. Mater. Chem. A*, 2014, **2**, 315-320.

79.   X. M. Chen, Z. X. Cai, X. Chen and M. Oyama, *J. Mater. Chem. A*, 2014, **2**, 5668-5674.

80.   Y. S. Feng, X. Y. Lin, J. Hao and H. J. Xu, *Tetrahedron*, 2014, **70**, 5249-5253.

81.   J. Qi, W. Lv, G. Zhang, Y. Li, G. Zhang, F. Zhang and X. Fan, *Nanoscale*, 2013, **5**, 6275-6279.

82.   N. Madhavan, C. W. Jones and M. Weck, *Acc. Chem. Res.*, 2008, **41**, 1153-1165.

83.   J. Y. Ji, G. H. Zhang, H. Y. Chen, S. L. Wang, G. L. Zhang, F. B. Zhang and X. B. Fan, *Chem. Sci.*, 2011, **2**, 484-487.

84.   F. J. Liu, J. Sun, L. F. Zhu, X. J. Meng, C. Z. Qi and F. S. Xiao, *J. Mater. Chem.*, 2012, **22**, 5495-5502.

85.   C. F. Yuan, W. F. Chen and L. F. Yan, *J. Mater. Chem.*, 2012, **22**, 7456-7460.

86.   W. F. Zhang, S. S. Wang, J. Y. Ji, Y. Li, G. L. Zhang, F. B. Zhang and X. B. Fan, *Nanoscale*, 2013, **5**, 6030-6033.

87.   W. F. Zhang, Q. S. Zhao, T. Liu, Y. Gao, Y. Li, G. L. Zhang, F. B. Zhang and X. B. Fan, *Ind. Eng. Chem. Res.*, 2014, **53**, 1437-1441.

88.   Y. Li, Q. S. Zhao, J. Y. Ji, G. L. Zhang, F. B. Zhang and X. B. Fan, *Rsc Adv.*, 2013, **3**, 13655-13658.

89.   Q. S. Zhao, D. F. Chen, Y. Li, G. L. Zhang, F. B. Zhang and X. B. Fan, *Nanoscale*, 2013, **5**, 882-885.

90.   Q. S. Zhao, Y. Li, R. Liu, A. Chen, G. L. Zhang, F. B. Zhang and X. B. Fan, *J. Mater. Chem. A*, 2013, **1**, 15039-15045.

91.   Q. S. Zhao, C. Bai, W. F. Zhang, Y. Li, G. L. Zhang, F. B. Zhang and X. B. Fan, *Ind. Eng. Chem. Res.*, 2014, **53**, 4232-4238.

92.   H. P. Cong, J. F. Chen and S. H. Yu, *Chem. Soc. Rev.*, 2014, **43**, 7295-7325.

93.   Z. H. Tang, S. L. Shen, J. Zhuang and X. Wang, *Angew. Chem. Int. Ed.*, 2010, **49**, 4603-4607.

94.   Y. C. Si and E. T. Samulski, *Chem.Mater.*, 2008, **20**, 6792-6797.

95.   C. G. Hu, H. H. Cheng, Y. Zhao, Y. Hu, Y. Liu, L. M. Dai and L. T. Qu, *Adv. Mater.*, 2012, **24**, 5493-5498.

96.   Z. S. Wu, S. B. Yang, Y. Sun, K. Parvez, X. L. Feng and K. Müllen, *J. Ame. Chem.Soc.*, 2012, **134**, 9082-9085.

97.   Y. Ma, M. G. Zhao, B. Cai, W. Wang, Z. Z. Ye and J. Y. Huang, *Biosens Bioelectron*, 2014, **59**, 384-388.

98.   X. C. Dong, X. W. Wang, L. H. Wang, H. Song, H. Zhang, W. Huang and P. Chen, *Acs Appl. Mater. Inter.*, 2012, **4**, 3129-3133.

99.   W. W. Cai, R. D. Piner, F. J. Stadermann, S. Park, M. A. Shaibat, Y. Ishii, D. X. Yang, A. Velamakanni, S. J. An, M. Stoller, J. H. An, D. M. Chen and R. S. Ruoff, *Science*, 2008, **321**, 1815-1817.

100.   W. Gao, L. B. Alemany, L. J. Ci and P. M. Ajayan, *Nat. Chem.*, 2009, **1**, 403-408.

101.   C. Gomez-Navarro, J. C. Meyer, R. S. Sundaram, A. Chuvilin, S. Kurasch, M. Burghard, K. Kern and U. Kaiser, *Nano Lett.*, 2010, **10**, 1144-1148.

102.   W. S. Hummers and R. E. Offeman, *J. Am. Chem. Soc.*, 1958, **80**, 1339-1339.

103.   D. R. Dreyer, H. P. Jia and C. W. Bielawski, *Angew. Chem. Int. Ed.*, 2010, **49**, 6813-6816.

104.   D. R. Dreyer and C. W. Bielawski, *Adv. Fun. Mater.*, 2012, **22**, 3247-3253.

105.   D. W. Boukhvalov, D. R. Dreyer, C. W. Bielawski and Y. W. Son, *Chemcatchem*, 2012, **4**, 1844-1849.

106.   S. B. Tang and Z. X. Cao, *Phys. Chem. Chem. Phys.*, 2012, **14**, 16558-16565.

107.   Y. J. Song, K. G. Qu, C. Zhao, J. S. Ren and X. G. Qu, *Adv. Mater.*, 2010, **22**, 2206-2210.

108. J. H. Yang, G. Sun, Y. J. Gao, H. B. Zhao, P. Tang, J. Tan, A. H. Lu and D. Ma, *Energ. Environ. Sci.*, 2013, **6**, 793-798.

109. D. M. Wang, Y. Zhang, L. L. Zheng, X. X. Yang, Y. Wang and C. Z. Huang, *J. Phys.Chem. C*, 2012, **116**, 21622-21628.

110. D. A. Heller, H. Jin, B. M. Martinez, D. Patel, B. M. Miller, T. K. Yeung, P. V. Jena, C. Hobartner, T. Ha, S. K. Silverman and M. S. Strano, *Nat. Nanotechnol.*, 2009, **4**, 114-120.

111. Y. J. Gao, D. Ma, C. L. Wang, J. Guan and X. H. Bao, *Chem.Commun.* 2011, **47**, 2432-2434.

112. D. H. Deng, L. Yu, X. L. Pan, S. Wang, X. Q. Chen, P. Hu, L. X. Sun and X. H. Bao, *Chem. Commun.*, 2011, **47**, 10016-10018.

113. C. L. Su, M. Acik, K. Takai, J. Lu, S. J. Hao, Y. Zheng, P. P. Wu, Q. L. Bao, T. Enoki, Y. J. Chabal and K. P. Loh, *Nat. Commun.*, 2012, **3**, 1298.

114. H. Q. Sun, S. Z. Liu, G. L. Zhou, H. M. Ang, M. O. Tade and S. B. Wang, *Acs Appl. Mater. Inter.*, 2012, **4**, 5466-5471.

115. A. Dhakshinamoorthy, M. Alvaro, P. Concepcion, V. Fornes and H. Garcia, *Chem. Commun.*, 2012, **48**, 5443-5445.

116. A. Dhakshinamoorthy, M. Alvaro, M. Puche, V. Fornes and H. Garcia, *Chemcatchem*, 2012, **4**, 2026-2030.

117. D. C. Wei, Y. Q. Liu, Y. Wang, H. L. Zhang, L. P. Huang and G. Yu, *Nano Lett.*, 2009, **9**, 1752-1758.

118. L. Y. Feng, Y. G. Chen and L. Chen, *Acs Nano*, 2011, **5**, 9611-9618.

119. H. Kim, K. Lee, S. I. Woo and Y. Jung, *Phys. Chem. Chem. Phys.*, 2011, **13**, 17505-17510.

120. Z. Q. Luo, S. H. Lim, Z. Q. Tian, J. Z. Shang, L. F. Lai, B. MacDonald, C. Fu, Z. X. Shen, T. Yu and J. Y. Lin, *J. Mater. Chem.*, 2011, **21**, 8038-8044.

121. Y. W. Ma, L. Y. Sun, W. Huang, L. R. Zhang, J. Zhao and Q. L. Fan, *J. Phys. Chem. C*, 2011, **115**, 24592-24597.

122. Z. H. Sheng, L. Shao, J. J. Chen, W. J. Bao, F. B. Wang and X. H. Xia, *Acs Nano*, 2011, **5**, 4350-4358.

123. S. B. Yang, X. L. Feng, X. C. Wang and K. Müllen, *Angew. Chem. Int. Ed.*, 2011, **50**, 5339-5343.

124. L. Yu, X. L. Pan, X. M. Cao, P. Hu and X. H. Bao, *J. Catal.*, 2011, **282**, 183-190.

125. L. P. Zhang and Z. H. Xia, *J. Phys. Chem. C*, 2011, **115**, 11170-11176.

126. D. W. Boukhvalov and Y. W. Son, *Nanoscale*, 2012, **4**, 417-420.

127. L. F. Lai, J. R. Potts, D. Zhan, L. Wang, C. K. Poh, C. H. Tang, H. Gong, Z. X. Shen, L. Y. Jianyi and R. S. Ruoff, *Energ. Environ. Sci.*, 2012, **5**, 7936-7942.

128. J. Liang, Y. Jiao, M. Jaroniec and S. Z. Qiao, *Angew. Chem. Int. Ed.*, 2012, **51**, 11496-11500.

129. J. L. Long, X. Q. Xie, J. Xu, Q. Gu, L. M. Chen and X. X. Wang, *Acs Catal.*, 2012, **2**, 622-631.

130. Z. Yang, Z. Yao, G. F. Li, G. Y. Fang, H. G. Nie, Z. Liu, X. M. Zhou, X. Chen and S. M. Huang, *Acs Nano*, 2012, **6**, 205-211.

131. Z. Yao, H. G. Nie, Z. Yang, X. M. Zhou, Z. Liu and S. M. Huang, *Chem. Commun.*, 2012, **48**, 1027-1029.

132. M. Y. Yen, C. K. Hsieh, C. C. Teng, M. C. Hsiao, P. I. Liu, C. C. M. Ma, M. C. Tsai, C. H. Tsai, Y. R. Lin and T. Y. Chou, *Rsc Adv.*, 2012, **2**, 2725-2728.

133. W. A. Saidi, *J. Phys. Chem. Lett.*, 2013, **4**, 4160-4165.

134. Y. Zheng, Y. Jiao, L. Ge, M. Jaroniec and S. Z. Qiao, *Angew. Chem. Int. Ed.*, 2013, **52**, 3110-3116.

135. C. H. Choi, H. K. Lim, M. W. Chung, J. C. Park, H. Shin, H. Kim and S. I. Woo, *J. Am. Chem. Soc.*, 2014, **136**, 9070-9077.

136. W. H. He, C. H. Jiang, J. B. Wang and L. H. Lu, *Angew. Chem. Int. Ed.*, 2014, **53**, 9503-9507.

137. S. Kattel, P. Atanassov and B. Kiefer, *J. Mater. Chem. A*, 2014, **2**, 10273-10279.

138. T. Xing, Y. Zheng, L. H. Li, B. C. C. Cowie, D. Gunzelmann, S. Z. Qiao, S. M. Huang and Y. Chen, *Acs Nano*, 2014, **8**, 6856-6862.

139. X. Wang, G. Sun, P. Routh, D.-H. Kim, W. Huang and P. Chen, *Chem. Soc. Rev.*, 2014, **43**, 7067-7098.

140. P. Wang, Z. K. Wang, L. X. Jia and Z. L. Xiao, *Phys. Chem. Chem. Phys.*, 2009, **11**, 2730-2740.

141. S. Y. Wang, L. P. Zhang, Z. H. Xia, A. Roy, D. W. Chang, J. B. Baek and L. M. Dai, *Angew. Chem. Int. Ed.*, 2012, **51**, 4209-4212.